Anomalous second-order skin modes in Floquet non-Hermitian systems

Chun-Hui Liu,[1] Haiping Hu,[2,3] Shu Chen,[2,3,4] and Xiong-Jun Liu [5,6,7,8,*]

[1]*Department of Physics, The University of Texas at Dallas, Richardson, Texas 75080-3021, USA*
[2]*Beijing National Laboratory for Condensed Matter Physics, Institute of Physics, Chinese Academy of Sciences, Beijing 100190, China*
[3]*School of Physical Sciences, University of Chinese Academy of Sciences, Beijing 100049, China*
[4]*Yangtze River Delta Physics Research Center, Liyang, Jiangsu 213300, China*
[5]*International Center for Quantum Materials and School of Physics, Peking University, Beijing 100871, China*
[6]*Hefei National Laboratory, Hefei 230088, China*
[7]*International Quantum Academy, Shenzhen 518048, China*
[8]*CAS Center for Excellence in Topological Quantum Computation, University of Chinese Academy of Sciences, Beijing 100190, China*

The non-Hermitian skin effect under open boundary conditions is widely believed to originate from the intrinsic spectral topology under periodic boundary conditions. If the eigenspectra under periodic boundary conditions have no spectral windings (e.g., piecewise arcs) or a finite area on the complex plane, there will be no non-Hermitian skin effect with open boundaries. In this article, we demonstrate another scenario beyond this perception by introducing a two-dimensional periodically driven model. The effective Floquet Hamiltonian lacks intrinsic spectral topology and is proportional to the identity matrix (representing a single point on the complex plane) under periodic boundary conditions. Yet, the Floquet Hamiltonian exhibits a second-order skin effect that is robust against perturbations and disorder under open boundary conditions. We further reveal the dynamical origin of these second-order skin modes and illustrate that they are characterized by a dynamical topological invariant of the full time-evolution operator.

I. INTRODUCTION

Non-Hermitian physics has recently garnered significant research interest. Many classical optical and mechanical systems, electric circuits, open quantum systems, and single-particle Green functions with nonzero self-energy are described by non-Hermitian Hamiltonians or matrices [1,2]. Several unique features of non-Hermitian systems have been discovered, including PT symmetry [3–12], the non-Hermitian skin effect [13–18], and exceptional points [19–29]. These unique features lead to a variety of tantalizing effects and phenomena in non-Hermitian systems without Hermitian counterparts [30–39]. Non-Hermitian systems have much richer topological phases [40,41], as exemplified by the 38-fold symmetry classes for time-independent point gap topology [42,43], and 54-fold symmetry classes for time-independent line gap topology and time-dependent systems [44,45].

In previous studies, the paradigmatic non-Hermitian skin effect has been attributed to the spectral topology under periodic boundary conditions. Specifically, in the complex-energy plane, the appearance of skin modes with open boundaries depends on the existence of spectral winding [46,47] or finite spectral area [48] under periodic boundary conditions. The skin modes can be categorized into different orders, where the nth-order ($n \leqslant d$) skin effect in d-dimensional systems

with L^d lattice sites indicates that the number of accumulated eigenstates at the $(d-n)$-dimensional boundary scales as $O(L^{d-n+1})$ [49–51]. The appearance of skin modes necessitates the introduction of a generalized Brillouin zone, through which the usual bulk-edge correspondence can be restored. And it is widely believed that the non-Hermitian skin effect (NHSE) is original from spectral winding.

In the Floquet Hermitian system, some papers have illustrated that topologically protected edge states can exist, even when the periodic boundary condition Floquet Hamiltonian is the identity matrix or indicates no topological edge modes [52–54]. The topological Floquet systems are called anomalous Floquet topological insulator (AFTI), which is beyond the theory of static topological insulators. Inspired by the AFTI, we propose a question: Is there any Floquet system where second-order NHSE can occur, even if the periodic boundary condition Floquet Hamiltonian is an identity matrix or indicates no second-order skin effect? We call it the anomalous Floquet second-order skin effect (AFSSE).

A rigorous theorem is the following: There is no NHSE for a finite Hilbert space Floquet Hermitian system. It means that some attempts based on a finite Hilbert space Floquet Hermitian Hamiltonian cannot get AFSSE [55,56], although the edge-effective model is the Hatano-Nelson model. To get the AFSSE, we need to introduce non-Hermitian terms. The topological classification of the Floquet non-Hermitian systems has been presented in Ref. [45]. The nonzero topological number in Table I of Ref. [45] indicates that there
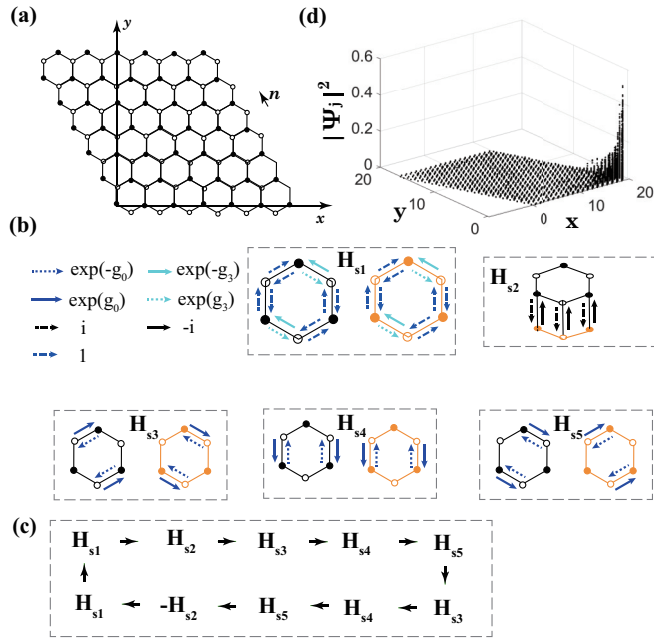
FIG. 1. Schematics of the model (top view) and driving protocol. (a) Honeycomb lattice with A (filled circles) and B (open circles) sublattices. (b) Non-Hermitian Hamiltonian H_{sj} ($j = 1, 2, \ldots, 5$) with nonreciprocal hoppings (marked by different lines) between neighboring sites. Black bonds and sites represent the top layer and the orange bonds and sites represent the bottom layer. (c) The 10-step driving sequence starting from H_{s1}. (d) Spatial profiles of the eigenstates. The parameters are $g_0 = 0.2$ and $t_1 = 0$. The system size is $L \times L = 20 \times 20$.

can be AFTI phases in the correspondence symmetry class and dimensions. In the two-dimensional AFTI phases, if the adjacent boundaries' effective Floquet operators both have NHSE and are localized at the same corner, then the corner coupling of the adjacent boundaries does not break the NHSE. This idea provides a method to construct the AFSSE.

This article presents a scheme that transcends the previous perception. As proof of principle, we introduce a two-dimensional Floquet driving system whose Floquet Hamiltonian is proportional to the identity matrix and has no intrinsic spectral topology. However, the Floquet Hamiltonian exhibits the second-order non-Hermitian skin effect with open boundaries. Furthermore, we demonstrate the robustness of these skin modes against perturbations and disorders and delve into their dynamical origins by explicitly working out the edge theory. We show that the skin modes are characterized by a dynamical topological invariant from the full time-evolution operator.

II. MODEL

We consider a bilayer hexagonal lattice structure [see Fig. 1(a)] and a 10-step Floquet driving sequence $H_{s1} \to H_{s2} \to \cdots \to H_{s10}$. The nth time step inside a driving period is governed by the time-independent Hamiltonian H_{sn}. We set $H_{s6} = H_{s3}$, $H_{s7} = H_{s4}$, $H_{s8} = H_{s5}$, $H_{s9} = -H_{s2}$,

$H_{s10} = H_{s1}$. They are given by

$$H_{s1}(\mathbf{k}) = \begin{bmatrix} H_A & 0 \\ 0 & H_A \end{bmatrix}, \quad H_{s2}(\mathbf{k}) = \begin{bmatrix} 0 & -i\mathbb{I} \\ i\mathbb{I} & 0 \end{bmatrix},$$

$$H_{s3}(\mathbf{k}) = \begin{bmatrix} H_1(\mathbf{k}, g_0) & 0 \\ 0 & H_3(\mathbf{k}, g_0) \end{bmatrix},$$

$$H_{s4}(\mathbf{k}) = \begin{bmatrix} H_2(\mathbf{k}, g_0) & 0 \\ 0 & H_2(\mathbf{k}, g_0) \end{bmatrix},$$

$$H_{s5}(\mathbf{k}) = \begin{bmatrix} H_3(\mathbf{k}, g_0) & 0 \\ 0 & H_1(\mathbf{k}, g_0) \end{bmatrix}, \tag{1}$$

where

$$H_1(\mathbf{k}, g) = \begin{bmatrix} 0 & e^{g+i\mathbf{k}\cdot\mathbf{a}_1} \\ e^{-g-i\mathbf{k}\cdot\mathbf{a}_1} & 0 \end{bmatrix},$$

$$H_2(\mathbf{k}, g) = \begin{bmatrix} 0 & e^{-g+i\mathbf{k}\cdot\mathbf{a}_2} \\ e^{g-i\mathbf{k}\cdot\mathbf{a}_2} & 0 \end{bmatrix}, \tag{2}$$

$$H_3(\mathbf{k}, g) = \begin{bmatrix} 0 & e^{-g+i\mathbf{k}\cdot\mathbf{a}_3} \\ e^{g-i\mathbf{k}\cdot\mathbf{a}_3} & 0 \end{bmatrix},$$

$$H_A = H_1(\mathbf{k}, g_1) + H_2(\mathbf{k}, g_2) + H_3(\mathbf{k}, g_3). \tag{3}$$

Here, g_0, g_1, g_2, g_3 are tunable nonreciprocal parameters between neighboring lattice sites. $\mathbf{a}_1 = (-\frac{a}{2}, -\frac{a}{2\sqrt{3}})$, $\mathbf{a}_2 = (0, \frac{a}{\sqrt{3}})$, and $\mathbf{a}_3 = (\frac{a}{2}, -\frac{a}{2\sqrt{3}})$ ($a = 1$ is the lattice constant). $\mathbf{k}$ is the lattice momentum and $\mathbb{I}$ is the identity matrix. The time duration for each step is denoted as $t_1, t_2, \ldots, t_{10}$, respectively. In this paper, we set $t_j = t_{11-j}$ for $j = 1, 2, 3, 4, 5$ and $g_1 = g_2 = 0$. Figures 1(b) and 1(c) sketch the nonreciprocal Hamiltonians in each step and the Floquet driving protocol.

The above driven system fulfills a type-K symmetry in the generalized Bernard-LeClair (GBL) class,

$$H(\mathbf{k}, t) = KH^*(-\mathbf{k}, -t)K^{-1}, \quad KK^* = -\mathbb{I}, \tag{4}$$

set by the driving protocol $H_{sj}(\mathbf{k}, t) = KH^*_{s11-j}(-\mathbf{k}, -t)K^{-1}$ ($j = 1, 2, 3, 4, 5$). Here, $K = \sigma_y \otimes \mathbb{I}$ (σ_y is Pauli matrix). The Floquet operator (U) is defined as the time-evolution operator in one full period $T = \sum_{j=1}^{10} t_j$,

$$U = e^{-iH_{s10}t_{10}} e^{-iH_{s9}t_9} \cdots e^{-iH_{s1}t_1}. \tag{5}$$

The Floquet Hamiltonian is the effective static Hamiltonian that stroboscopically tracks the time evolution. It is defined as $H_F = \frac{i}{T}\ln(U)$. We always take $t_2 = t_3 = t_4 = t_5 = \frac{\pi}{2}$ in this article, unless otherwise stated.

Notably, when $t_1 = 0$, the time-evolution operator is easily solvable and given simply by $U(\mathbf{k}) = -\mathbb{I}$, with the corresponding bulk Floquet Hamiltonian being $H_F(\mathbf{k}) = \frac{\pi}{T}\mathbb{I}$. Surprisingly, there are $O(L)$ eigenstates located at one single corner under the open boundary condition, while the other eigenstates are extended across the whole system, as shown in Fig. 1(d) for $g_3 = 0.2$. These localized states are known as the second-order skin modes and have previously been associated with the eigenspectra of a finite area on the complex plane or topological properties [49–51] of the bulk Hamiltonian under periodic boundary conditions. However, in this model, the spectra of the Floquet Hamiltonian represent only a single
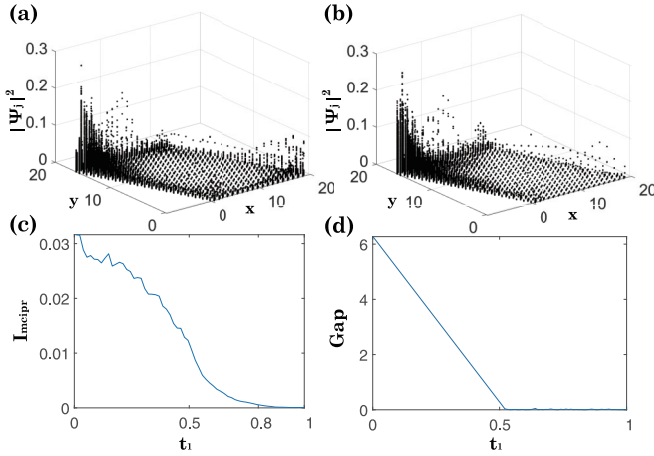
FIG. 2. Stability of second-order skin modes against perturbations. Spatial profiles of all eigenstates $|\psi_j(\mathbf{r}, 1)|^2$ and $|\psi_j(\mathbf{r}, 2)|^2$ for (a) $t_1 = 0.8$ and (b) $t_1 = 1$. (c) MCIPR as a function of t_1. (d) Bulk spectral gap as a function of t_1. The open boundary is taken along $\mathbf{a}_3$ and its perpendicular direction. The non-Bloch band theory is used to obtain the bulk spectra. The system size is $L \times L = 20 \times 20$. $g_0 = 0.2$ and $g_3 = -0.4$.

point on the complex plane, without any topological structure or spectral area. Therefore, this model lacks any static counterparts and a complete understanding of the appearance of these skin modes requires an account of the full-time evolution.

III. PERTURBATION AND DISORDER

Next, we demonstrate the robustness of the second-order skin effect against perturbations (i.e., deviating from the ideal case described above.) We introduce a nonzero value for parameter t_1 and investigate the interplay between the first- and second-order skin effects. Additionally, we show that the second-order skin effect is resistant to disorder: the skin modes survive even in the presence of significant disorder strength.

A. Perturbation

Let us deviate from the ideal case of Fig. 1 and take $g_3 = -0.4$, $t_1 = 0.8$ with other parameters unchanged. Figure 2(a) plots the spatial profiles of the eigenstates $|\psi_j(\mathbf{r}, 1)|$ and $|\psi_j(\mathbf{r}, 2)|$ $(j = 1, 2, \ldots, 4L^2 - 4)$ with open boundary condition. Here, $z = 1$ or 2 denotes the top or bottom layer, j labels the eigenstate, and $\mathbf{r} = (x, y)$ labels the lattice site. It is clear that there are $O(L)$ eigenvectors located at the bottom right corner and $O(L^2)$ eigenvectors located at the top left corner. That is, the first-order skin modes start to emerge, while the second-order skin modes persist. When t_1 increases to 1, all eigenvectors are located at the top left corner, as depicted in Fig. 2(b).

To scrutinize the second-order skin effect, we define a partial inverse partition ratio of eigenvector $\psi_j(\mathbf{r}, z)$,

$$I_{\text{cipr}}(j) = \frac{\sum_{\mathbf{r} \in \mathcal{A}}[|\psi_j(\mathbf{r}, 1)|^4 + |\psi_j(\mathbf{r}, 2)|^4]}{\sum_{\mathbf{r}}[|\psi_j(\mathbf{r}, 1)|^2 + |\psi_j(\mathbf{r}, 2)|^2]}. \tag{6}$$

It has support on the bottom right part of the lattice sites with $\mathcal{A} = \{(x, y)|(x + \sqrt{3}y) > \frac{\sqrt{3}(L+1)}{2}, y < \frac{\sqrt{3}(L-1)}{4}\}$. We dub it as the corner inverse partition ratio (CIPR) and define the mean CIPR (MCIPR) over all eigenstates as

$$I_{\text{mcipr}} = \frac{\sum_j I_{\text{cipr}}(j)}{4L^2 - 4}. \tag{7}$$

In Fig. 2(c), the quantity I_{mcipr} is plotted as a function of t_1. The decrease in I_{mcipr} with increasing t_1 is due to the emergence of first-order skin modes and the growth of the localization length for the second-order skin modes. The small jittering in the plot may be due to finite-size effects or the in-cell wave functions' relative changes with the variation of t_1. In a broad range of values for t_1, both first-order and second-order skin modes can be found, localized on different corners. However, as t_1 increases beyond a certain threshold, the first-order skin effect dominates, suppressing the second-order skin modes and pulling them towards the top left corner, as illustrated in Fig. 2(b). I_{mcipr} can be used as an order parameter and the threshold value is reached at around $t_1 = 0.9$, where all second-order skin modes have been eliminated (i.e., they have infinite localization length). To estimate the threshold value of I_{mcipr}, the presence of a few extended states and the rest being localized first-order skin modes is assumed. The critical value of I_{mcipr} scales as $I_{\text{mcipr}} \propto 1/(16L^2)$, where L is the system size. In Fig. 2(d), the Floquet Hamiltonian real gap at 0 of the bulk states [45] is plotted as a function of t_1. The Floquet Hamiltonian real gap is defined as the real line gap of H_F. Here, we take open boundary conditions along $\mathbf{a}_3$ and its perpendicular direction and utilize the non-Bloch band theory (or generalized Brillouin zone) to obtain the bulk spectra. The gap decreases and closes around $t_1 = 0.5$, indicating a bulk topological transition that will be discussed later.

Consider directions $\mathbf{a}_3$ and $\mathbf{b}_1 = (\frac{a}{2\sqrt{3}}, \frac{a}{2})$; there is no NHSE if we take the open boundary condition (OBC) for the $\mathbf{b}_1$ direction and periodic boundary condition (PBC) for the $\mathbf{a}_3$ direction. It means that the bulk spectrum is not dependent on the boundary conditions in the $\mathbf{b}_1$ direction for $L \to \infty$. The bulk spectrum of the open $\mathbf{b}_1$ and $\mathbf{a}_3$ directions is equivalent to the bulk spectrum of the open $\mathbf{a}_3$ direction and PBC on the $\mathbf{b}_1$ direction. Taking the Fourier transformation for the $\mathbf{b}_1$ direction, the bulk spectrum of the open $\mathbf{a}_3$ direction and PBC on the $\mathbf{b}_1$ direction transforms into a one-dimensional problem. Thus, we can use the one-dimensional non-Bloch band theory to get the spectrum. It is similar to case A in Ref. [57], which also does not have NHSE in one direction.

If $t_1 = 0$, $H_F(\mathbf{k}) = \frac{\pi}{T}\mathbb{I}$. If $t_1 \neq 0$, $H_F(\mathbf{k}) = H_{s1}(\mathbf{k}) + \frac{\pi}{T}\mathbb{I}$. In Ref. [49], Kawabata et al. found that there is a topological number defined by the Hamiltonian under PBC that has correspondence with second-order skin modes. After Fourier transforms $H_F(\mathbf{k})$ to real space, there is no second-order skin effect in both the $t_1 = 0$ and $t_1 \neq 0$ regions under OBC. Thus, there is no topological number defined by $H_F(\mathbf{k})$ that has correspondence with second-order skin modes for our model.

In Ref. [55], they study the Hermitian Rudner-Lindner-Berg-Levin (RLBL) model. They found that the edge-effective Floquet operator of the RLBL model is the Hatano-Nelson model. After cutting a hopping bound

of the Hatano-Nelson model, the NHSE occurs for the Hatano-Nelson model. The significant point is that there is no NHSE in the two-dimensional cut hopping bound RLBL model. The cutting bound and getting edge-effective Floquet operator is not commutable. A rigorous theorem prohibits the existence of NHSE for the Floquet operator of the finite Hilbert space Hermitian system: There is no NHSE for the Floquet operator of finite Hilbert space Hermitian systems. The eigenstates of the finite Hilbert space unitary operator U are the same as the eigenstates of $\ln(U)$. $\ln(U)$ is a finite Hilbert space Hermitian operator. According to the theorem, for a Hermitian operator with finite Hilbert space, its eigenstates are orthogonal to each other, thus the eigenstates of the finite Hilbert space unitary operator are also orthogonal to each other. The Floquet operator of the finite Hilbert space Hermitian system is a finite Hilbert space unitary operator; its eigenstates are also orthogonal to each other. If the Floquet operator of the finite Hilbert space Hermitian system has NHSE, there will be $O(L^{d_1})$ eigenstates located at d_2-dimensional boundary with $d_1 > d_2$, which means that the eigenstates cannot be orthogonal to each other. It is not consistent with the fact that the eigenstates of the Floquet operator of the finite Hilbert space Hermitian system are orthogonal to each other. Thus, we get that there is no NHSE for the Floquet operator of finite Hilbert space Hermitian systems. The models discussed in Refs. [55,56] both belong to finite Hilbert space Hermitian Floquet systems. Thus, there is no NHSE in their models, although their models' edge-effective Floquet operator is the Hatano-Nelson model. Our models belong to non-Hermitian Floquet systems, which is beyond the control of this theorem. That is the reason why our model can have NHSE.

Another method mentioned in Ref. [49] to understand the second-order skin modes is to relate second-order skin modes with the spectral of the edge states under OBC in one direction and PBC in another direction. If there is a loop in the PBC's (only one direction) edge spectra, a second-order skin effect may exist. This method is not rigorous and works well in many cases. For the model in Sec. IV A of Ref. [45], there is a loop in the PBC's (only PBC in one direction) edge spectra, and there is no second-order skin effect. In Sec. IV, we give the effective edge theory of this model for $t_1 = 0$ (the exactly solvable limit). The effective-edge theory gives an intuitive understanding of the second-order skin modes. For $t_1 \neq 0$, we give a topological invariant which is defined by the full time-evolution operator protecting the second-order skin modes. The topological invariant reveals that the second-order skin effect is the origin from anomalous Floquet topology, which may exist even for the PBC's Floquet Hamiltonian that is proportional to the identity matrix. This origin leads to that the usual understanding of the second-order skin effect in time-independent systems cannot be used to understand this model's second-order skin effect (there is no anomalous Floquet topology for the time-independent system).

B. Disorder

Now let us consider the effect of disorder and take $t_1 = \pi/20$, $g_0 = 0.2$, and $g_3 = 0$. We add a time-independent
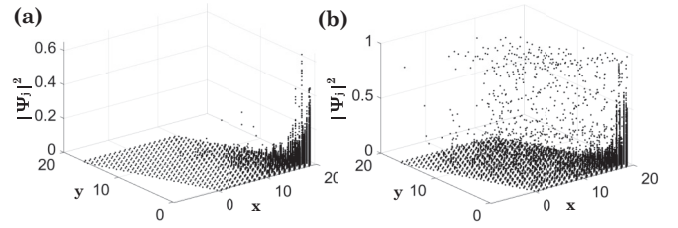

FIG. 3. Robustness of second-order skin modes with respect to disorder. Spatial profiles of all eigenstates $|\psi_j(\mathbf{r}, 1)|^2$ and $|\psi_j(\mathbf{r}, 2)|^2$ for disorder strength (a) $W_D = 1$ and (b) $W_D = 100$. Other parameters are $t_1 = \pi/20$, $g_0 = 0.2$, and $g_3 = 0$. The system size is $L \times L = 20 \times 20$.

disorder H_{diso} to each step of the system's Hamiltonian,

$$H_{\text{diso}} = \sum_{\mathbf{r}}[w_d(\mathbf{r})a_{\mathbf{r},1}^\dagger a_{\mathbf{r},1} + w_d(\mathbf{r})a_{\mathbf{r},2}^\dagger a_{\mathbf{r},2}], \quad (8)$$

where $a_{\mathbf{r},z}^\dagger$, $a_{\mathbf{r},z}$ ($z = 1, 2$) are creation and annihilation operations on the $\mathbf{r}$ lattice site in the z layer, respectively. $w_d(\mathbf{r})$ is a random variable with constant probability distribution in the interval $[-W_D, W_D]$. $w_d(\mathbf{r}_i)$ and $w_d(\mathbf{r}_j)$ ($\mathbf{r}_i \neq \mathbf{r}_j$) are independent of each other. Figures 3(a) and 3(b) plot the spatial profiles of $|\psi_j(\mathbf{r}, 1)|$ and $|\psi_j(\mathbf{r}, 2)|$ ($j = 1, 2, \ldots, 4L^2 - 4$) with $W_D = 1$ and $W_D = 100$, respectively. We can see that the second-order skin modes persist in a broad region of disorder strength and coexist with Anderson localization states.

IV. EDGE THEORY AND TOPOLOGICAL NUMBER

A major advantage of our model is that it is analytically solvable under certain conditions, e.g., in the absence of disorder and $t_1 = 0$. This would greatly help us to gain an intuitive understanding of the emergence of second-order skin modes. For this case, the bulk Floquet operator is trivial. However, we have nontrivial edge states which are dynamically induced and the Floquet operator of the top, bottom, left, and right edges (denoted as U_T, U_B, U_L, and U_R, respectively) are

$$\begin{aligned} U_L = \sum_n \frac{1}{2}[e^{-4g_0}(a_{uA,n+2}^\dagger - a_{dA,n+2}^\dagger)a_{uA,n} \\ + e^{4g_0}(a_{uA,n}^\dagger - a_{dA,n}^\dagger)a_{uA,n+2} \\ + e^{-4g_0}(-a_{uA,n+2}^\dagger + a_{dA,n+2}^\dagger)a_{dA,n} \\ + e^{4g_0}(a_{uA,n}^\dagger + a_{dA,n}^\dagger)a_{dA,n+2}] \\ - \sum_n(a_{uB,n}^\dagger a_{uB,n} + a_{dB,n}^\dagger a_{dB,n}), \quad (9) \end{aligned}$$

$$\begin{aligned} U_R = \sum_n \frac{1}{2}[e^{4g_0}(a_{uB,n}^\dagger - a_{dB,n}^\dagger)a_{uB,n+2} \\ + e^{-4g_0}(a_{uB,n+2}^\dagger - a_{dB,n+2}^\dagger)a_{uB,n} \\ - e^{4g_0}(-a_{uB,n}^\dagger - a_{dB,n}^\dagger)a_{dB,n+2} \\ + e^{-4g_0}(a_{uB,n+2}^\dagger + a_{dB,n+2}^\dagger)a_{dB,n}] \\ - \sum_n(a_{uA,n}^\dagger a_{uA,n} + a_{dA,n}^\dagger a_{dA,n}), \quad (10) \end{aligned}$$

$$U_T = \sum_x \frac{1}{2}[e^{4g_0}(a^\dagger_{uB,x+2} - a^\dagger_{dB,x+2})a_{dB,x}$$

$$+ e^{-4g_0}(a^\dagger_{uB,x} + a^\dagger_{dB,x})a_{uB,x+2}$$

$$- e^{4g_0}(-a^\dagger_{uB,x+2} - a^\dagger_{dB,x+2})a_{dB,x}$$

$$+ e^{-4g_0}(a^\dagger_{uB,x} + a^\dagger_{dB,x})a_{dB,x+2}]$$

$$- \sum_x (a^\dagger_{uA,x}a_{uA,x} + a^\dagger_{dA,x}a_{dA,x}), \qquad (11)$$

$$U_B = \sum_x \frac{1}{2}[e^{-4g_0}(a^\dagger_{uA,x} - a^\dagger_{dA,x})a_{uA,x+2}$$

$$+ e^{4g_0}(a^\dagger_{uA,x+2} + a^\dagger_{dA,x+2})a_{uA,x}$$

$$- e^{-4g_0}(a^\dagger_{uA,x} - a^\dagger_{dA,x})a_{dA,x+2}$$

$$+ e^{4g_0}(a^\dagger_{uA,x+2} + a^\dagger_{dA,x+2})a_{dA,x}]$$

$$- \sum_x (a^\dagger_{uB,x}a_{uB,x} + a^\dagger_{dB,x}a_{dB,x}). \qquad (12)$$

Here, $a^\dagger_{zm,x}$ and $a_{zm,x}$ ($z = u, d$ and $m = A, B$) are the creation and annihilation operators on the z layer, xth unit cell, and m sublattice. x is the cell index along the **x** direction [see Fig. 1(a)]. u and d represent the 1 and 2 layer, respectively. Similarly, $a^\dagger_{zm,n}$ and $a_{zm,n}$ are the creation and annihilation operators on the z layer, nth unit cell, and m site, respectively. n is the cell index along the **n** direction [see Fig. 1(a)]. Fourier transform of Eqs. (9)–(12) brings us to the momentum space and we have

$$U_L = \sum_{k_1} A^\dagger_{k_1} \begin{bmatrix} L_A & 0 \\ 0 & -\mathbb{I} \end{bmatrix} A_{k_1},$$

$$U_R = \sum_{k_1} A^\dagger_{k_1} \begin{bmatrix} -\mathbb{I} & 0 \\ 0 & R_B \end{bmatrix} A_{k_1},$$

$$U_T = \sum_{k_2} B^\dagger_{k_2} \begin{bmatrix} -\mathbb{I} & 0 \\ 0 & T_B \end{bmatrix} B_{k_2},$$

$$U_B = \sum_{k_2} B^\dagger_{k_2} \begin{bmatrix} D_A & 0 \\ 0 & -\mathbb{I} \end{bmatrix} B_{k_2}. \qquad (13)$$

Here,

$$L_A = \frac{1}{2}\begin{bmatrix} e^{-4g-2ik_1} + e^{4g+2ik_1} & -e^{-4g-2ik_1} + e^{4g+2ik_1} \\ -e^{-4g-2ik_1} + e^{4g+2ik_1} & e^{-4g-2ik_1} + e^{4g+2ik_1} \end{bmatrix},$$

$$R_B = \frac{1}{2}\begin{bmatrix} e^{-4g-2ik_1} + e^{4g+2ik_1} & -e^{-4g-2ik_1} + e^{4g+2ik_1} \\ -e^{-4g-2ik_1} + e^{4g+2ik_1} & e^{-4g-2ik_1} + e^{4g+2ik_1} \end{bmatrix},$$

$$T_B = \frac{1}{2}\begin{bmatrix} e^{4g-2ik_2} + e^{-4g+2ik_2} & -e^{4g-2ik_2} + e^{-4g+2ik_2} \\ -e^{4g-2ik_2} + e^{-4g+2ik_2} & e^{4g-2ik_2} + e^{-4g+2ik_2} \end{bmatrix},$$

$$D_A = \frac{1}{2}\begin{bmatrix} e^{4g-2ik_2} + e^{-4g+2ik_2} & -e^{4g-2ik_2} + e^{-4g+2ik_2} \\ -e^{4g-2ik_2} + e^{-4g+2ik_2} & e^{4g-2ik_2} + e^{-4g+2ik_2} \end{bmatrix}. \qquad (14)$$

In our notation, $A_{k_1} = [a_{uAk_1}, a_{dAk_1}, a_{uBk_1}, a_{dBk_1}]$, $B_{k_2} = [a_{uAk_2}, a_{dAk_2}, a_{uBk_2}, a_{dBk_2}]$, $a_{zmn} = \sum_{k_1} e^{ik_1 n} a_{zmk_1}$, and $a_{zmx} = \sum_{k_2} e^{ik_2 x} a_{zmk_2}$, $z = u, d$ and $m = A, B$. k_1 and k_2 are the momenta along the **n** and **x** directions, respectively. The above edge Floquet operators can be considered as similar to the Hatano-Nelson model, with nonreciprocal hoppings. When a full open boundary is applied in both directions, the eigenvectors of U_L and U_R are situated along the bottom edges, while the eigenvectors of U_T and U_B are located on the right edges. The combination of these edge Floquet operators results in the accumulation of edge states at the bottom right corner of all eigenvectors.

While the second-order skin effect can be intuitively understood through these effective-edge Floquet operators, the stability of these skin modes and their origin are encoded in a dynamical topological invariant, as discussed below. For convenience, we denote $U(\mathbf{k}, t)$ as the time-evolution operator of this model. According to Table I of Ref. [45], this model belongs to the GBL class K2a and has $\mathbb{Z}_2$ topological classification. For Floquet systems, the description of the system's topological properties needs to take into account its micromotion operator $\tilde{U} = U(\mathbf{k}, t) * e^{iH_F t}$, in which the $*$ operator is defined in Ref. [45]. A Hermitianization procedure is then applied and the associated Hermitian operator is defined as

$$H_{\tilde{U}} = \begin{bmatrix} 0 & \tilde{U}(\mathbf{k}, t) \\ \tilde{U}(\mathbf{k}, t)^\dagger & 0 \end{bmatrix}. \qquad (15)$$

By treating time t as another momentum, the Hamiltonian $H_{\tilde{U}}$ can be classified as belonging to the three-dimensional Hermitian CII class [58,59]. The derivation of the symmetries of $H_{\tilde{U}}$ is given in Ref. [45]. It should be noted that whether or not $U(k, t)$ is unitary, the $H_{\tilde{U}}$ is always Hermitian and belongs to class CII. Denoting $|\psi_\alpha\rangle$ ($\alpha = 1, 2, 3, 4$) as the occupied eigenstates of $H_{\tilde{U}}$ with negative eigenenergies, the non-Abelian Berry connection is defined as

$$A^{\alpha,\beta}(\mathbf{k}, t) = \langle \psi_\alpha | \nabla_\mathbf{k} \psi_\beta \rangle \cdot d\mathbf{k} + \langle \psi_\alpha | \nabla_t \psi_\beta \rangle \cdot dt. \qquad (16)$$

The desired $\mathbb{Z}_2$ topological invariant is then the second Chern-Simons topological number $W_{CS} = \text{CS} \bmod 2$ with [58,59]

$$\text{CS} = \frac{-1}{8\pi^2} \int_{BZ \times t \in [0,T]} \text{Tr}\left[AdA + \frac{2}{3}A^3\right]. \qquad (17)$$

Our numerical calculations show that $W_{CS} = 1$ before the gap closure in Fig. 2(d), while it is not well defined after the gap closure. The Chern-Simons topological number dictates the existence of topologically protected helical edge states. The nonreciprocal couplings along the boundaries collapse them into second-order skin modes under full open boundary conditions.

A special case worth mentioning is when $t_2 = 0$ and $t_3 = t_4 = t_5 = \pi/2$. In this case, the two layers are decoupled and each layer reduces to a previously studied model (Sec. IV A of Ref. [45]). The topological invariants of the layers are given by three-dimensional winding numbers, with values of 1 and -1, respectively. These winding numbers dictate the existence of topological edge states for each layer. If we take periodic boundary conditions along the **x** direction and open boundary conditions along the **n** direction, the type-K symmetry enforces a twofold degeneracy (for the real part)
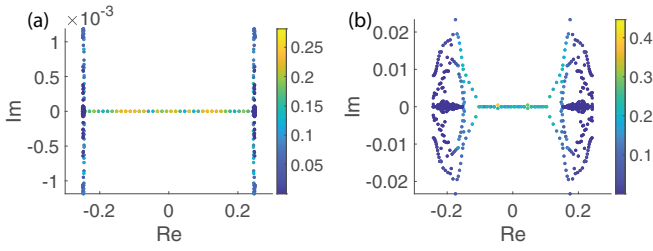
FIG. 4. OBC spectrum of H_F for parameters set as $g_0 = 0.2$ and $g_3 = -0.4$. System size $L \times L = 20 \times 20$. The color represents the I_{cipr} of the corresponding eigenstate. (a) $t_1 = 0.01$ and (b) $t_1 = 0.2$.

at $k = \pi$ at the top and bottom edges (see Appendix A for details). As long as the real gap of the Floquet Hamiltonians persists, this degeneracy cannot be removed. Therefore, the topological edge states are stable and protected by the Floquet Hamiltonian's real gap, even when we deviate from the special case (e.g., by tuning t_1 and t_2 to nonzero values).

Here, we demonstrate the stability of the second-order skin modes. The second-order skin modes cannot hybridize with first-order skin modes as long as the W_{CS} is nonzero. Figures 4(a) and 4(b) are the spectrum of the OBC's H_F for $t_1 = 0.01$ and $t_1 = 0.2$, respectively [other parameters are the same as in Fig. 2(a)]. And the color in Figs. 4(a) and 4(b) represents the I_{cipr} of the corresponding eigenstate. $W_{CS} = 1$ for Figs. 4(a) and 4(b), which means that there are topologically protected real line gapless states for the OBC's H_F. According to Figs. 4(a) and 4(b), we can get that the second-order skin modes correspond to topologically protected edge states. And the first-order skin modes and extended states correspond to bulk states. Thus, the second-order skin modes cannot hybridize with first-order skin modes as long as the W_{CS} is nonzero.

To get a well-defined W_{CS}, we requires the symmetry given by Eq. (4) and the real line gap at 0 for Floquet Hamiltonian H_F [45]. As long as the perturbations are much less than the real line gap of H_F at 0, the gap cannot close by adding the perturbations. Thus, we can regard the perturbation as a weak perturbation. Otherwise, we can regard the perturbation as a strong perturbation. On the other hand, according to the numerical results in Sec. III B, the second-order skin effect is stable against disorder, given by Eq. (8). The disorder given by Eq. (8) fulfills the symmetry, given by Eq. (4), and almost breaks all other symmetries. The numerical results illustrate that the second-order skin effect is stable and consistent with the second-order skin modes being protected by W_{CS}.

V. GENERALIZATION AND REALIZATION

One potential implementation of our model and driving protocol (in GBL class K2a) is through the two-dimensional unitary random walk (RW), a widely used platform of Floquet topological phases. The recipe of our setup is the anomalous Floquet topological insulator in class A [60]. By coupling two such RWs with opposite three-winding numbers $(+1$ and $-1)$, we can obtain an anomalous Floquet topological insulator in class AII. To implement the non-Hermitian terms in the Floquet operators, we utilize polarization-dependent

photon gain/loss, which respects type-K symmetry [61]. The appearance of second-order skin modes in this setup should be confirmed by observing pronounced photon localizations near one of the system corners. Another possible platform for implementing our model is through open systems. A more detailed discussion of this approach can be found in Appendix B.

VI. CONCLUSIONS

In conclusion, we have demonstrated the emergence of second-order skin modes in a two-dimensional Floquet driving system, where the bulk Floquet band is trivially flat and characterized by an identity Floquet operator $-\mathbb{I}$. Our scheme surpasses prior knowledge that the non-Hermitian skin effect only arises from intrinsic bulk topology or the finite spectral area under periodic boundary conditions in the static systems. Additionally, we have shown that these second-order skin modes are robust against perturbations and disorders. We have further revealed the topological origin of these skin modes from the edge theory and the Chern-Simons dynamical topological invariant. Generalization to high-dimensional systems or other symmetry classes will be left for future study.

APPENDIX A: PROOF OF THE REAL-PART DEGENERACY OF THE FLOQUET SPECTRA AT HIGH SYMMETRY POINT WITH TYPE-K SYMMETRY: $H(\mathbf{k}, t) = KH^*(-\mathbf{k}, -t)K^{-1}, \ KK^* = -\mathbb{I}$

The type-K symmetry is

$$H(\mathbf{k}, t) = KH^*(-\mathbf{k}, -t)K^{-1}, \quad KK^* = -\mathbb{I}. \quad \text{(A1)}$$

According to Eq. (20) of Ref. [45], the Floquet operator fulfills

$$[U^*(-\mathbf{k})]^{-1} = K^{-1}U(\mathbf{k})K, \quad KK^* = -\mathbb{I}. \quad \text{(A2)}$$

It follows that the eigenfunction $\psi_j(\mathbf{k})$ and eigenenergy $E_j(\mathbf{k})$ of $U(\mathbf{k})$ [$E_j(\mathbf{k}) = \rho_j(\mathbf{k})e^{i\theta_j(\mathbf{k})}, \rho_j(\mathbf{k}) > 0, 0 \leqslant \theta_j(\mathbf{k}) < 2\pi$] satisfy

$$U(\mathbf{k})\psi_j(\mathbf{k}) = E_j(\mathbf{k})\psi_j(\mathbf{k}). \quad \text{(A3)}$$

Thus, we have

$$E_j(\mathbf{k})\psi_j(\mathbf{k}) = U(\mathbf{k})\psi_j(\mathbf{k}) = K[U^*(-\mathbf{k})]^{-1}K^{-1}\psi_j(\mathbf{k})$$

$$\Longleftrightarrow \quad E_j(\mathbf{k})K^{-1}\psi_j(\mathbf{k}) = [U^*(-\mathbf{k})]^{-1}K^{-1}\psi_j(\mathbf{k})$$

$$\Longleftrightarrow \quad E_j(\mathbf{k})U^*(-\mathbf{k})K^{-1}\psi_j(\mathbf{k}) = K^{-1}\psi_j(\mathbf{k})$$

$$\Longleftrightarrow U(-\mathbf{k})(K^*)^{-1}\psi_j^*(\mathbf{k}) = [E_j(\mathbf{k})^*]^{-1}(K^*)^{-1}\psi_j^*(\mathbf{k}). \quad \text{(A4)}$$

At high symmetry point $\mathbf{k}_0$ ($\mathbf{k}_0 = -\mathbf{k}_0$), we have

$$U(\mathbf{k}_0)(K^*)^{-1}\psi_j^*(\mathbf{k}_0) = [E_j(\mathbf{k}_0)^*]^{-1}(K^*)^{-1}\psi_j^*(\mathbf{k}_0). \quad \text{(A5)}$$

The Floquet Hamiltonian at k_0 is $H_F(\mathbf{k}_0) = \frac{i}{T}\ln[U(\mathbf{k}_0)]$. Here we choose the imaginary part of the $\ln(\cdot)$ function to be in the $[0, 2\pi)$ interval. Note that both $\psi_j(\mathbf{k}_0)$ and $(K^*)^{-1}\psi_j^*(\mathbf{k}_0)$ are eigenfunctions of $H_F(\mathbf{k}_0)$, with their associated eigenenergies $\frac{1}{T}\{\ln[\rho_j(\mathbf{k}_0)]i - \theta_j(\mathbf{k}_0)\}$ and $\frac{1}{T}\{-\ln[\rho_j(\mathbf{k}_0)]i - \theta_j(\mathbf{k}_0)\}$. If $\psi_j(\mathbf{k}_0)$ and $(K^*)^{-1}\psi_j^*(\mathbf{k}_0)$ are not degenerate (with the same real part of eigenenergies), we have

$$\psi_j(\mathbf{k}_0) = e^{i\delta}(K^*)^{-1}\psi_j^*(\mathbf{k}_0). \quad \text{(A6)}$$

Thus,

$$(K^*)^{-1}\psi_j^*(\mathbf{k}_0) = (K^*)^{-1}[e^{i\delta}(K^*)^{-1}\psi_j^*(\mathbf{k}_0)]^* = -e^{-i\delta}\psi_j(\mathbf{k}_0) \quad \text{(A7)}$$

$$\Longleftrightarrow \quad \psi_j(\mathbf{k}_0) = -e^{i\delta}(K^*)^{-1}\psi_j^*(\mathbf{k}_0), \quad \text{(A8)}$$

which contradicts Eq. (A6). Therefore, $\psi_j(\mathbf{k}_0)$ and $(K^*)^{-1}\psi_j^*(\mathbf{k}_0)$ are degenerate eigenfunctions (with the same real part of eigenenergies).

APPENDIX B: REALIZATION OF THE MODEL IN OPEN QUANTUM SYSTEMS

Let us consider Markovian open quantum systems, which are described by the Lindblad equation

$$\frac{d\rho}{dt} = \mathcal{L}[\rho] = -i[H, \rho] + \sum_\mu (2L_\mu \rho L_\mu^\dagger - \{L_\mu^\dagger L_\mu, \rho\}), \quad \text{(B1)}$$

where ρ is the density matrix, H is the systems' Hamiltonian, and L_μ is the Lindblad operator. They are all time dependent. Similarly to Appendix D of Ref. [32], if each Lindblad operator is a linear combination of annihilate operators, we have

$$|\langle 0|(a_{j_2}(t)a_{j_1}^\dagger(0) + a_{j_1}^\dagger(0)a_{j_2}(t))|0\rangle|^2 = |\langle 0|a_{j_2}(t)a_{j_1}^\dagger(0)|0\rangle|^2$$

$$= |\langle 0|e^{\mathcal{L}(\Delta t)^\dagger \Delta t}[e^{\mathcal{L}(2\Delta t)^\dagger \Delta t}[\dots [e^{\mathcal{L}(t)^\dagger \Delta t}[a_{j_2}(0)]]\dots]]|j_1\rangle|^2$$

$$= |\text{Tr}[e^{\mathcal{L}(\Delta t)^\dagger \Delta t}[e^{\mathcal{L}(2\Delta t)^\dagger \Delta t}[\dots [e^{\mathcal{L}(t)^\dagger \Delta t}[a_{j_2}(0)]]\dots]]|j_1\rangle\langle 0|]|^2$$

$$= |\text{Tr}[a_{j_2}(0)e^{\mathcal{L}(t)^\dagger \Delta t}[\dots [e^{\mathcal{L}(2\Delta t)^\dagger \Delta t}[e^{\mathcal{L}(\Delta t)^\dagger \Delta t}[|j_1\rangle\langle 0|]]]\dots]]|^2$$

$$= |\text{Tr}[a_{j_2}(0)e^{-iH_{\text{eff}}(t)\Delta t}\dots e^{-iH_{\text{eff}}(2\Delta t)\Delta t}e^{-iH_{\text{eff}}(\Delta t)\Delta t}|j_1\rangle\langle 0|]|^2$$

$$= |\text{Tr}[e^{-iH_{\text{eff}}(t)\Delta t}\dots e^{-iH_{\text{eff}}(2\Delta t)\Delta t}e^{-iH_{\text{eff}}(\Delta t)\Delta t}|j_1\rangle\langle 0|a_{j_2}(0)]|^2$$

$$= |\langle j_2|e^{-iH_{\text{eff}}(t)\Delta t}\dots e^{-iH_{\text{eff}}(2\Delta t)\Delta t}e^{-iH_{\text{eff}}(\Delta t)\Delta t}|j_1\rangle|^2. \quad \text{(B2)}$$

Here, $H_{\text{eff}}(t) = H(t) - i\sum_\mu^L L_\mu^{l\dagger}(t)L_\mu^l(t)$, and $L_\mu^l(t)$ is a time-dependent Lindblad operator which is a linear combination of the annihilate operator. $j_1 = (\mathbf{r}_1, z_1, m_1)$ and $j_2 = (\mathbf{r}_2, z_2, m_2)$, $\mathbf{r}_1$ and $\mathbf{r}_2$ are the two dimensional coordinates, $z_1, z_2 = 1, 2$ are the layer index, and $m_1, m_1 = A, B$ are the sublattice index. The single-particle evolution is governed by $H_{\text{eff}}(t)$. Thus, we can construct a 10-step driven open quantum system to realize the model in the main text. The Hamiltonian and Lindblad operators in each step are

$$h_1 = \sum_{\mathbf{r}, z=1,2} (a_{\mathbf{r},zA}^\dagger a_{\mathbf{r}+\mathbf{a}_1,zB} + a_{\mathbf{r}+\mathbf{a}_1,zB}^\dagger a_{\mathbf{r},zA} + a_{\mathbf{r},zA}^\dagger a_{\mathbf{r}+\mathbf{a}_2,zB} + a_{\mathbf{r}+\mathbf{a}_2,zB}^\dagger a_{\mathbf{r},zA} + \beta_3 a_{\mathbf{r},zA}^\dagger a_{\mathbf{r}+\mathbf{a}_3,zB} + \beta_3 a_{\mathbf{r}+\mathbf{a}_3,zB}^\dagger a_{\mathbf{r},zA}),$$

$$L_{\mathbf{r},1}^1 = \sqrt{\gamma_3}(a_{\mathbf{r},1A} - ia_{\mathbf{r}+\mathbf{a}_3,1B}),$$

$$L_{\mathbf{r},2}^1 = \sqrt{\gamma_3}(a_{\mathbf{r},1A} - ia_{\mathbf{r}+\mathbf{a}_3,1B}),$$

$$h_2 = \sum_{\mathbf{r}} (a_{\mathbf{r},1A}^\dagger a_{\mathbf{r},2A} + a_{\mathbf{r},1B}^\dagger a_{\mathbf{r},2B} + \text{H.c.}),$$

$$h_3 = \sum_{\mathbf{r}} \beta_0 (a_{\mathbf{r},1A}^\dagger a_{\mathbf{r}+\mathbf{a}_1,1B} + a_{\mathbf{r}+\mathbf{a}_1,1B}^\dagger a_{\mathbf{r},1A} + a_{\mathbf{r},2A}^\dagger a_{\mathbf{r}+\mathbf{a}_3,2B} + a_{\mathbf{r}+\mathbf{a}_3,2B}^\dagger a_{\mathbf{r},2A}),$$

$$L_{\mathbf{r},1}^3 = \sqrt{\gamma_0}(a_{\mathbf{r}+\mathbf{a}_1,1B} - ia_{\mathbf{r},1A}),$$

$$L_{\mathbf{r},2}^3 = \sqrt{\gamma_0}(-ia_{\mathbf{r}+\mathbf{a}_3,2B} + a_{\mathbf{r},2A}),$$

$$h_4 = \sum_{\mathbf{r}} \beta_0 (a_{\mathbf{r},1A}^\dagger a_{\mathbf{r}+\mathbf{a}_2,1B} + a_{\mathbf{r}+\mathbf{a}_2,1B}^\dagger a_{\mathbf{r},1A} + a_{\mathbf{r},2A}^\dagger a_{\mathbf{r}+\mathbf{a}_2,2B} + a_{\mathbf{r}+\mathbf{a}_2,2B}^\dagger a_{\mathbf{r},2A}),$$

$$L_{\mathbf{r},1}^4 = \sqrt{\gamma_0}(a_{\mathbf{r}+\mathbf{a}_2,1B} - ia_{\mathbf{r},1A}),$$

$$L_{\mathbf{r},2}^4 = \sqrt{\gamma_0}(a_{\mathbf{r}+\mathbf{a}_2,2B} - ia_{\mathbf{r},2A}),$$

$$h_5 = \sum_{\mathbf{r}} \beta_0(a_{\mathbf{r},1A}^\dagger a_{\mathbf{r}+\mathbf{a}_3,1B} + a_{\mathbf{r}+\mathbf{a}_3,1B}^\dagger a_{\mathbf{r},1A} + a_{\mathbf{r},2A}^\dagger a_{\mathbf{r}+\mathbf{a}_1,2B} + a_{\mathbf{r}+\mathbf{a}_1,2B}^\dagger a_{\mathbf{r},2A}),$$

$$L_{\mathbf{r},1}^5 = \sqrt{\gamma_0}(a_{\mathbf{r},1A} - ia_{\mathbf{r}+\mathbf{a}_3,1B}),$$

$$L_{\mathbf{r},2}^5 = \sqrt{\gamma_0}(a_{\mathbf{r}+\mathbf{a}_1,2B} - ia_{\mathbf{r},2A}),$$

$$h_6 = h_3, \quad L_{\mathbf{r},1}^6 = L_{\mathbf{r},1}^3, \quad L_{\mathbf{r},2}^6 = L_{\mathbf{r},2}^3, \quad h_7 = h_4, \quad L_{\mathbf{r},1}^7 = L_{\mathbf{r},1}^4, \quad L_{\mathbf{r},2}^7 = L_{\mathbf{r},2}^4,$$

$$h_8 = h_5, \quad L_{\mathbf{r},1}^8 = L_{\mathbf{r},1}^5, \quad L_{\mathbf{r},2}^8 = L_{\mathbf{r},2}^5, \quad h_9 = -h_2, \quad h_{10} = h_1, \quad L_{\mathbf{r},1}^{10} = L_{\mathbf{r},1}^1, \quad L_{\mathbf{r},2}^{10} = L_{\mathbf{r},2}^1. \tag{B3}$$

Here, $\mathbf{r}$ is the two-dimensional coordinate, and $a_{\mathbf{r},zm}^\dagger$ and $a_{\mathbf{r},zm}$ ($z = 1, 2$ and $m = A, B$) are the creation and annihilation operators on the $\mathbf{r}$ cell, zth layer, and m site. $\beta_0 = \frac{1}{2}(e^{-g_0} + e^{g_0})$, $\gamma_0 = \frac{1}{2}(e^{g_0} - e^{-g_0})$, $\beta_3 = \frac{1}{2}(e^{-g_3} + e^{g_3})$, and $\gamma_3 = \frac{1}{2}(e^{g_3} - e^{-g_3})$. The driven sequences in one period are

$$\begin{aligned}(h_1, L_{\mathbf{r},z}^1) &\rightarrow (h_2, 0) \rightarrow (h_3, L_{\mathbf{r},z}^3) \rightarrow (h_4, L_{\mathbf{r},z}^4) \rightarrow (h_5, L_{\mathbf{r},z}^5) \\ &\rightarrow (h_6, L_{\mathbf{r},z}^6) \rightarrow (h_7, L_{\mathbf{r},z}^7) \rightarrow (h_8, L_{\mathbf{r},z}^8) \rightarrow (h_9, 0) \\ &\rightarrow (h_{10}, L_{\mathbf{r},z}^{10}).\end{aligned} \tag{B4}$$

The driven time for each step is t_1, t_2,..., t_{10}, respectively. According to Eq. (B2), for this system we have

$$\begin{aligned}&|\langle 0|[a_{j_2}(T)a_{j_1}^\dagger(0) + a_{j_1}^\dagger(0)a_{j_2}(T)]|0\rangle|^2 \\ &= |\langle 0|a_{j_2}(T)a_{j_1}^\dagger(0)|0\rangle|^2\end{aligned}$$

$$= |\langle j_2|e^{-i\hat{H}_{s10}t_{10}} \ldots e^{-i\hat{H}_{s2}t_2} e^{-i\hat{H}_{s1}t_1}|j_1\rangle|^2. \tag{B5}$$

Except for the shift by a constant matrix, $\hat{H}_{s1}, \hat{H}_{s2}, \ldots, \hat{H}_{s1}$ take the form of $H_{s1}, H_{s2}, \ldots H_{s10}$ in momentum space, respectively (under the basis $A_B = [a_{\mathbf{k},1A}, a_{\mathbf{k},1B}, a_{\mathbf{k},2A}, a_{\mathbf{k},2B}]$). Going beyond the static limit and using the conclusions in Refs. [30,62,63], or Appendix A of Ref. [31], the Green function

$$\Delta_{\mathbf{r}_1 z_1 m_1, \mathbf{r}_2 z_2 m_2}(t) = \mathrm{Tr}[\rho(t)a_{\mathbf{r}_1 z_1 m_1}^\dagger a_{\mathbf{r}_2 z_2 m_2}] \tag{B6}$$

satisfies

$$\begin{aligned}\Delta(nT) = {}&e^{-2n\mathbb{I}(\gamma_3 t_1 + \gamma_0(t_3 + t_4 + t_5))}(e^{-iH_{s10}t_{10}} \ldots e^{-iH_{s2}t_2} e^{-iH_{s1}t_1})^n \\ &\times \Delta(0)(e^{iH_{s1}^\dagger t_1} e^{iH_{s2}^\dagger t_2} \ldots e^{iH_{s10}^\dagger t_{10}})^n,\end{aligned} \tag{B7}$$

where $\mathbb{I}$ is the identity matrix and n is a positive integer. According to Eq. (B7), the many-particle dynamics is also governed by the model in the main text.

[1] Y. Ashida, Z. Gong, and M. Ueda, Adv. Phys. **69**, 249 (2020).

[2] E. J. Bergholtz, J. C. Budich, and F. K. Kunst, Rev. Mod. Phys. **93**, 015005 (2021).

[3] C. M. Bender and S. Boettcher, Phys. Rev. Lett. **80**, 5243 (1998).

[4] C. M. Bender, D. C. Brody, and H. F. Jones, Phys. Rev. Lett. **89**, 270401 (2002).

[5] S. Longhi, Phys. Rev. Lett. **103**, 123601 (2009).

[6] Y. C. Hu and T. L. Hughes, Phys. Rev. B **84**, 153101 (2011).

[7] A. Regensburger, C. Bersch, M.-A. Miri, G. Onishchukov, D. N. Christodoulides, and U. Peschel, Nature (London) **488**, 167 (2012).

[8] L. Feng, Z. J. Wong, R.-M. Ma, Y. Wang, and X. Zhang, Science **346**, 972 (2014).

[9] B. Zhu, R. Lü, and S. Chen, Phys. Rev. A **89**, 062102 (2014).

[10] C. Yuce, Eur. Phys. J. D **69**, 184 (2015).

[11] Y. Ashida, S. Furukawa, and M. Ueda, Nat. Commun. **8**, 15791 (2017).

[12] R. El-Ganainy, K. G. Makris, M. Khajavikhan, Z. H. Musslimani, S. Rotter, and D. N. Christodoulides, Nat. Phys. **14**, 11 (2018).

[13] T. E. Lee, Phys. Rev. Lett. **116**, 133903 (2016).

[14] S. Yao and Z. Wang, Phys. Rev. Lett. **121**, 086803 (2018).

[15] F. K. Kunst, E. Edvardsson, J. C. Budich, and E. J. Bergholtz, Phys. Rev. Lett. **121**, 026808 (2018).

[16] S. Lieu, Phys. Rev. B **97**, 045106 (2018).

[17] C.-X. Guo, C.-H. Liu, X.-M. Zhao, Y. Liu, and S. Chen, Phys. Rev. Lett. **127**, 116801 (2021).

[18] Z.-Y. Wang, J.-S. Hong, and X.-J. Liu, Phys. Rev. B **108**, L060204 (2023).

[19] H. Shen, B. Zhen, and L. Fu, Phys. Rev. Lett. **120**, 146402 (2018).

[20] B. Zhen, C. W. Hsu, Y. Igarashi, L. Lu, I. Kaminer, A. Pick, S.-L. Chua, J. D. Joannopoulos, and M. Soljačić, Nature (London) **525**, 354 (2015).

[21] J. Doppler, A. A. Mailybaev, J. Böhm, U. Kuhl, A. Girschik, F. Libisch, T. J. Milburn, P. Rabl, N. Moiseyev, and S. Rotter, Nature (London) **537**, 76 (2016).

[22] H. Xu, D. Mason, L. Jiang, and J. Harris, Nature (London) **537**, 80 (2016).

[23] V. Kozii and L. Fu, arXiv:1708.05841.

[24] Y. Xu, S.-T. Wang, and L.-M. Duan, Phys. Rev. Lett. **118**, 045701 (2017).

[25] M. Papaj, H. Isobe, and L. Fu, Phys. Rev. B **99**, 201107(R) (2019).

[26] M.-A. Miri and A. Alù, Science **363**, eaar7709 (2019).

[27] C.-X. Guo, S. Chen, K. Ding, and H. Hu, Phys. Rev. Lett. **130**, 157201 (2023).

[28] H. Hu, S. Sun, and S. Chen, Phys. Rev. Res. **4**, L022064 (2022).

[29] K. Ding, C. Fang, and G. Ma, Nat. Rev. Phys. **4**, 745 (2022).

[30] F. Song, S. Yao, and Z. Wang, Phys. Rev. Lett. **123**, 170401 (2019).

[31] C.-H. Liu, K. Zhang, Z. Yang, and S. Chen, Phys. Rev. Res. **2**, 043167 (2020).

[32] C.-H. Liu and S. Chen, Phys. Rev. B **104**, 174305 (2021).

[33] H. Hu and E. Zhao, Phys. Rev. Lett. **126**, 010401 (2021).

[34] H. Hu, E. Zhao, and W. V. Liu, Phys. Rev. B **106**, 094305 (2022).

[35] J. Bartlett, H. Hu, and E. Zhao, Phys. Rev. B **104**, 195131 (2021).

[36] M. M. Denner, A. Skurativska, F. Schindler, M. H. Fisher, R. Thomale, T. Bzdušek, and T. Neupert, Nat. Commun. **12**, 5681 (2021).

[37] C.-X. Guo, X. Wang, H. Hu, and S. Chen, Phys. Rev. B **107**, 134121 (2023).

[38] B. Li, H.-R. Wang, F. Song, and Z. Wang, Phys. Rev. B **108**, L161409 (2023).

[39] P. Molignini, O. Arandes, and E. J. Bergholtz, Phys. Rev. Res. **5**, 033058 (2023).

[40] Z. Gong, Y. Ashida, K. Kawabata, K. Takasan, S. Higashikawa, and M. Ueda, Phys. Rev. X **8**, 031079 (2018).

[41] C.-H. Liu, H. Jiang, and S. Chen, Phys. Rev. B **99**, 125103 (2019).

[42] K. Kawabata, K. Shiozaki, M. Ueda, and M. Sato, Phys. Rev. X **9**, 041015 (2019).

[43] H. Zhou and J. Y. Lee, Phys. Rev. B **99**, 235112 (2019).

[44] C.-H. Liu and S. Chen, Phys. Rev. B **100**, 144106 (2019).

[45] C.-H. Liu, H. Hu, and S. Chen, Phys. Rev. B **105**, 214305 (2022).

[46] N. Okuma, K. Kawabata, K. Shiozaki, and M. Sato, Phys. Rev. Lett. **124**, 086801 (2020).

[47] K. Zhang, Z. Yang, and C. Fang, Phys. Rev. Lett. **125**, 126402 (2020).

[48] K. Zhang, Z. Yang, and C. Fang, Nat. Commun. **13**, 2496 (2022).

[49] K. Kawabata, M. Sato, and K. Shiozaki, Phys. Rev. B **102**, 205118 (2020).

[50] R. Okugawa, R. Takahashi, and K. Yokomizo, Phys. Rev. B **102**, 241202(R) (2020).

[51] D. Zou, T. Chen, W. He, J. Bao, C. H. Lee, H. Sun, and X. Zhang, Nat. Commun. **12**, 7201 (2021).

[52] M. S. Rudner, N. H. Lindner, E. Berg, and M. Levin, Phys. Rev. X **3**, 031005 (2013).

[53] R. Roy and F. Harper, Phys. Rev. B **96**, 155118 (2017).

[54] T. Kitagawa, E. Berg, M. Rudner, and E. Demler, Phys. Rev. B **82**, 235114 (2010).

[55] H. Liu and I. C. Fulga, Phys. Rev. B **108**, 035107 (2023).

[56] T. Bessho, K. Mochizuki, H. Obuse, and M. Sato, Phys. Rev. B **105**, 094306 (2022).

[57] K. Yokomizo and S. Murakami, Phys. Rev. B **107**, 195112 (2023).

[58] C.-K. Chiu, J. C. Y. Teo, A. P. Schnyder, and S. Ryu, Rev. Mod. Phys. **88**, 035005 (2016).

[59] J. C. Y. Teo and C. L. Kane, Phys. Rev. B **82**, 115120 (2010).

[60] C. Chen, X. Ding, J. Qin, Y. He, Y.-H. Luo, M.-C. Chen, C. Liu, X.-L. Wang, W.-J. Zhang, H. Li, L.-X. You, Z. Wang, D.-W. Wang, B. C. Sanders, C.-Y. Lu, and J.-W. Pan, Phys. Rev. Lett. **121**, 100502 (2018).

[61] L. Xiao, X. Zhan, Z. Bian, K. Wang, X. Zhang, X. Wang, J. Li, K. Mochizuki, D. Kim, N. Kawakami *et al.*, Nat. Phys. **13**, 1117 (2017).

[62] T. Prosen, New J. Phys. **10**, 043026 (2008).

[63] S. Diehl, A. Micheli, A. Kantian, B. Kraus, H. Büchler, and P. Zoller, Nat. Phys. **4**, 878 (2008).